

High Strength Discontinuously Reinforced Aluminum For Rocket Applications

A.B. Pandey¹, S.R. Shah², and M. Shadoan²

¹ Pratt & Whitney Space Propulsion, Materials & Processes Engineering,
West Palm Beach, Fl 33410.

² National Aeronautics and Space Administration, NASA Marshall Space Flight Center,
Huntsville, Al 35812.

Abstract

*Silicon-Carbide
Boron-Carbide*

This study presents results on the development of a new aluminum alloy with very high strength and ductility. Five compositions of Al-Mg-Sc-Gd-Zr alloy was selected for this purpose. These alloys were also reinforced with 15 volume percent (~~SiC~~) and (~~B₄C~~) particles to produce Discontinuously Reinforced Aluminum (DRA) materials. Matrix alloys and DRA were processed using a powder metallurgy process. The helium gas atomization produced very fine powder with cellular-dendritic microstructure. The microstructure of matrix alloys showed fine Al₃Sc based precipitate which provides significant strengthening in these alloys. DRA showed uniform distribution of reinforcement in aluminum matrix. DRA materials were tested at -320°F, 75°F in air and 75°F in gaseous hydrogen environments and matrix alloys were tested at 75°F in air. DRA showed high strengths in the range of 89-111 ksi (614-697 MPa) depending on alloy compositions and test environments. Matrix alloys had a good combination of strength, 84-89 ksi (579-621 MPa) and ductility, 4.5-6.5%. The properties of these materials can further be improved by proper control of processing parameters.

Introduction

Discontinuously reinforced aluminum (DRA) has found a number of applications in aerospace structures due to its higher specific modulus; specific strength and fatigue resistance compared to unreinforced aluminum alloys. In recent years, there has been growing interest in the development of DRA materials for rocket applications to improve the thrust to weight ratio of engines. DRA can potentially be used for components that experience a range of temperatures from cryogenic to 450°F. The existing DRA materials have limited strength at ambient and elevated temperatures. The strength of DRA is derived primarily from the strength of matrix alloys. The commercial DRA materials use medium strength, 6000 and 2000 series, aluminum alloys as matrices and therefore, strength is limited at ambient temperature. The strength at elevated temperatures degrades due to rapid coarsening of strengthening precipitates. Therefore, a new matrix alloy that can provide high strength at ambient and elevated temperatures is required.

Considerable work has been done in the past for developing high temperature aluminum alloys for applications at 600°F [1]. Among these alloys, Al-Fe-V-Si [2], Al-Fe-Ce [3], Al-Fe-Ce-W [4], Al-Fe-Mo-V [5], and Al-Cr-Zr-Mn [6] are the most notable. In addition, Al-Zr-V [7] and Al-Ti [8] were also investigated for such applications. Most of these alloys have incoherent dispersoids with volume fractions of 15-25 %. The strength of Al-Fe based alloys degraded considerably at higher temperatures due to coarsening of dispersoids [9] and the ductility of these alloys showed a dip at intermediate temperatures, 300-390°F [10-11]. The fracture toughness of most of these alloys is low, 7-14 ksiv in except for Al-Fe-V-Si which had toughness of 23-27 ksiv in [9]. Higher toughness of Al-Fe-V-Si was due to delamination at stringers of intermetallic particles [9]. The delamination may cause reduction in transverse strength and ductility of Al-Fe-V-Si alloy. None of these alloys qualified for applications due to considerable reduction in properties at elevated temperatures.

The present approach is based on the following criteria: (a) selection of alloying elements with low solid state diffusion rates and solid solubilities in aluminum, and (b) selection of alloying elements that can form $L1_2$ coherent precipitates with aluminum in the equilibrium condition. The coherent precipitates can provide improved thermal stability through a decrease in the interfacial energy. Scandium is known to be a potent strengthener in aluminum alloys [12]. Scandium forms coherent A_3Sc phase with aluminum in the equilibrium condition. The A_3Sc dispersoid has $L1_2$ type crystal structure and is thermally stable at elevated temperatures [13]. Considerable research has been conducted in Al-Sc alloys to understand the strengthening effect of A_3Sc precipitates [14-18]. Most studies have concentrated on Al-Sc alloys with Sc level up to 0.6 wt. % in casting due to its maximum solid solubility limit of 0.4 wt. %. The strengthening effect of Sc can be extended significantly by addition of higher Sc content. Higher Sc can be taken in supersaturation by using powder metallurgy processing with higher cooling rate. Limited studies on higher Sc containing alloys are available [19-20]. Unal and Kainer [20] have investigated Al-Mg-Sc alloy using powder processing that showed significantly higher strength compared to the lower Sc alloys. Pandey et al. [20] has evaluated the microstructure and tensile properties of Al-Mg-Sc-Zr alloy.

Gadolinium with aluminum forms eutectic mixture of Al solid solution and A_3Gd particles. Zirconium forms A_3Zr that has $L1_2$ structure similar to that of A_3Sc . The substitution of A_3Gd and A_3Zr is expected to occur in A_3Sc forming $A_3(Sc,Gd,Zr)$ phase. This phase is expected to be thermally stable and stronger than individual phases. The substitution of Gd and Zr will also reduce the Sc content that can reduce the cost of alloy. Magnesium was chosen to provide solid

solution strengthening, to increase the lattice parameter that can bring the lattice parameter of Al_3Sc and Al even closer, and to reduce the density of the alloy.

The goal of the overall program is to develop a new aluminum alloy to provide a balanced combination of high strength and ductility at ambient and elevated temperatures for rocket applications. The objective of the present study is to report preliminary data on microstructure and tensile properties of powder processed Al-Mg-Sc-Gd-Zr alloys with and without reinforcements.

Materials and Processing

For the present study, five different compositions of Al-Mg-Sc-Gd-Zr alloys were selected. The nominal compositions were as follows: Al-6Mg-2Sc (VX-11), Al-6Mg-2Sc-1Gd-1Zr (VX-12), Al-6Mg-1Sc-1.5Gd-0.5Zr (VX-13), Al-6Mg-1Sc-1Gd-1Zr (VX-14) Al-6Mg-1Sc-1Gd-0.5Zr (VX-15). The compositions are given in weight percent. Master alloys of Al-Sc, Al-Gd and Al-Zr were used for making alloys with target compositions. In order to minimize oxidation, melting of alloy was carried out in an inert atmosphere. The alloy was remelted and atomized using helium gas atomization to produce fine powder. Using helium gas for atomization minimized oxidation of powder. Powder was sieved to minus 325 mesh fraction using standard sieving procedure. SiC and B_4C particles were used at 15-volume percent level as reinforcement in aluminum matrix for making DRA materials. The aluminum alloy powder and reinforcement powder were blended together to provide a uniform distribution of reinforcement in the matrix. The unreinforced (matrix) Al alloy powder and DRA with SiC and B_4C particles were processed separately for consolidation to achieve full density. The powder was hot vacuum degassed to remove residual gas and water vapor. Consolidation of powder was carried out using vacuum hot pressing. The density of consolidated billets was close to theoretical density. Few billets had less than 100% density. Billets were extruded at 662°F using an extrusion ratio of 25:1 which produces round bars with 0.6" diameter. One of the matrix alloy compositions was extruded at 572, 662 and 752°F.

Atomized powder and extruded rods were examined for microstructures using optical microscopy and scanning electron microscopy (SEM). Back-scattered electron imaging was performed to reveal Al_3Sc -based dispersoid in aluminum. Tensile properties of extruded matrix alloy and DRA materials were determined at liquid nitrogen temperature; and at ambient temperature in air and gaseous hydrogen environments. Tensile tests were performed using MTS at a strain rate of $1.6 \times 10^{-4} \text{ s}^{-1}$. The fracture surfaces of matrix alloys and DRA were examined using secondary electron imaging.

Results and Discussion

The phase diagram of Al-Sc alloy is shown in Figure 1. The Al-Sc alloy forms eutectic at 0.5 wt.% of Sc with a mixture of solid solution Al and Al_3Sc . The eutectic temperature is 1218F (932K) with an extremely shallow α + liquid phase

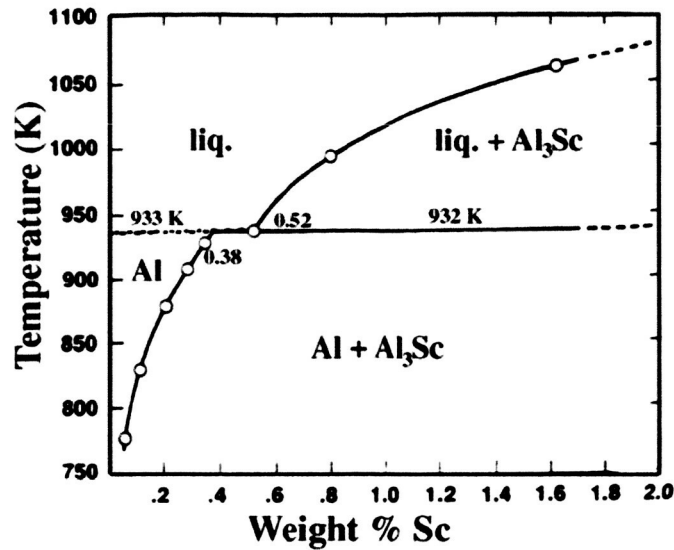
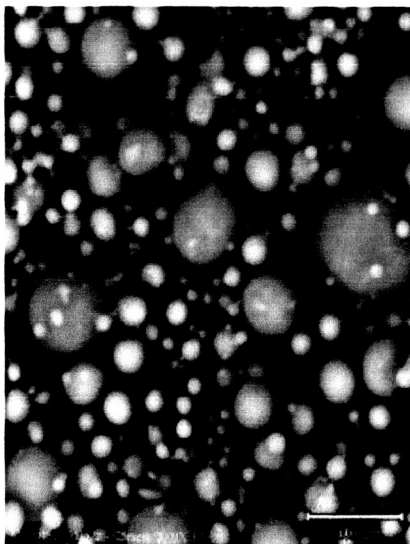
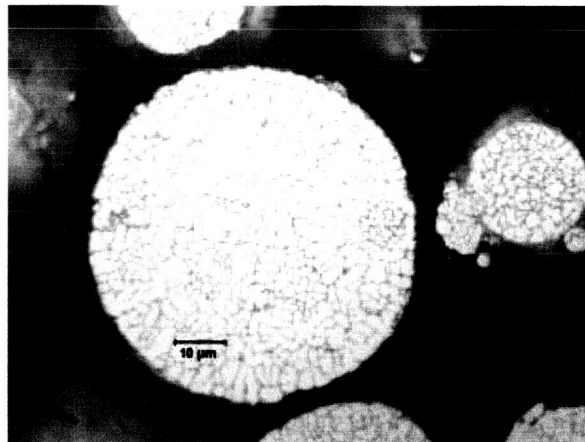


Figure 1: The Al-Sc phase diagram showing an extremely shallow Al + L phase field [21].

field and thus, narrow freezing range for hypoeutectic alloy compositions. For hypereutectic alloys, the large freezing range exists indicating that a higher cooling rate is required to suppress formation of large Al₃Sc particles. Figure 2(a) shows the SEM micrograph of atomized powder of VX-13 alloy. The powder is spherical in shape indicating good flowability of the powder. Spherical shape also indicates that the powder is clean and free from excessive oxidation. The spherical shape resulted from the inert gas used for melting and atomization of the alloy. Some satellites are also observed in the micrograph resulting from collision of a finer and coarser powder in flight during solidification stage. Finer particles solidify faster than coarser ones. Satellites are produced by collision of solidified fine particles with semisolid coarse particles. Excessive satellite particles can reduce the packing density of the powder.



(a)



(b)

Figure 2: (a) SEM micrograph of VX-13 alloy showing spherical powder produced by helium gas atomization and (b) cross-section of powder showing cellular microstructure.

Figure 2(b) shows an optical microstructure of powder cross-section indicating presence of cellular morphology. The size of cells can be used to determine the cooling rate experienced by the powder during atomization. There is a relation between size of powder, size of cells and the cooling rate. The cooling rate varies inversely with powder size. The cell size varies directly with powder size. The cooling rate of atomization ranges from 10^4 to 10^6 °F/s depending on the powder size.

Figure 3(a)&(b) shows the SEM micrograph of SiC and B₄C powders. Both powders have irregular shape with sharp corners. Irregular shape is typically observed for commercial grade SiC and B₄C powders. While this powder is normally used for making DRA due to easy availability and lower cost, the angular shape is not desired from ductility point of view.

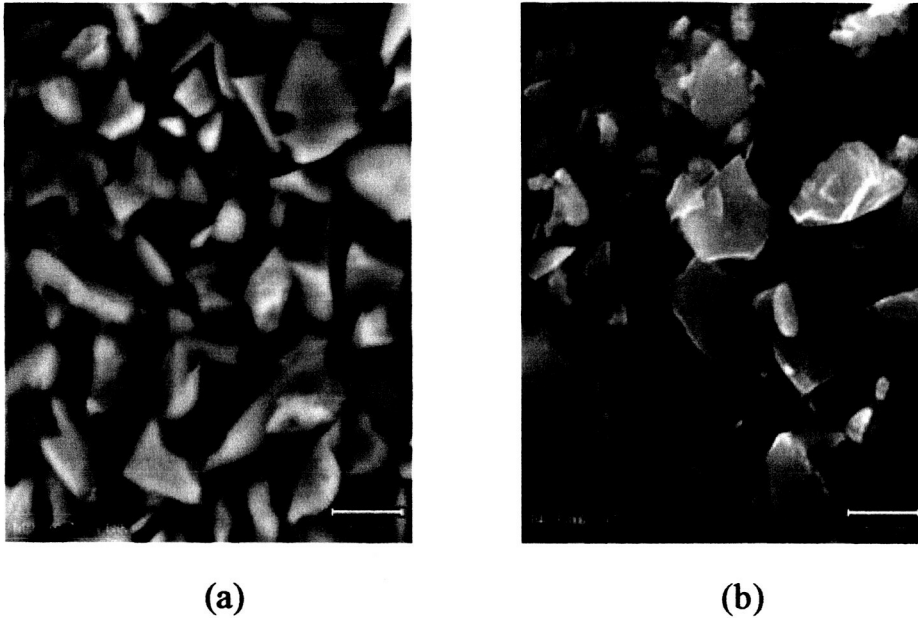


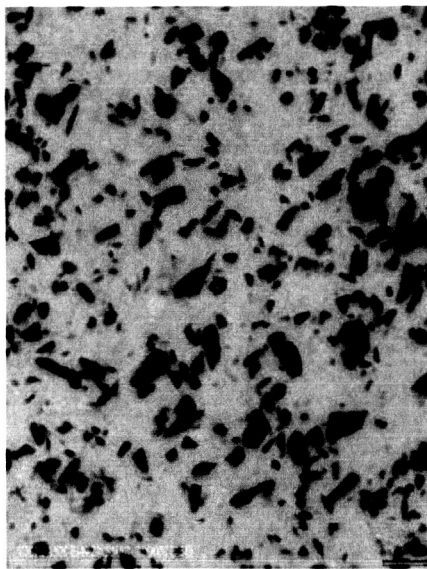
Figure 3: (a) SEM micrograph of SiC and (b) B₄C powders showing irregular shape

Table 1 includes the particle size analysis of aluminum alloy powders. The analysis indicates that 90% of powder is below 35 μm with average powder size about 10-14 μm depending on alloy compositions. The helium gas atomization with a suitable control of parameters produced powder not only with a fine average size but also with a narrow size distribution. A slight variation in the average size of powder is related with variation in atomization parameters. The size of powder is controlled by metal superheat, metal flow rate and velocity of atomizing gas.

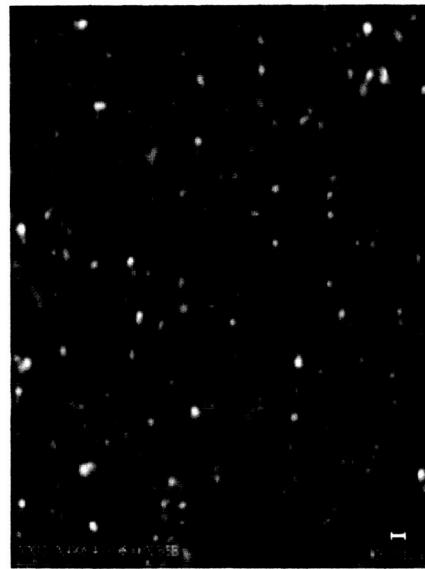
Figure 4(a) shows the back-scattered SEM microstructure of extruded DRA with SiC particles. The dark phase is SiC and light phase is aluminum matrix. Figure 4(b) shows SEM microstructure of matrix aluminum phase in DRA at high magnification to reveal very fine (100-200 nm) sized Al₃(Sc,Gd,Zr) precipitate. The Al₃Sc based precipitate appears to be formed during processing of powder as no post processing heat treatment has been given. This precipitate is expected to provide considerable strengthening in this material. These alloys are also expected to contain very fine, about 8 nm, Al₃Sc based precipitate similar to that reported earlier [22] that can provide significant strengthening to this material.

Table 1: Powder analysis showing very fine average size

Alloys ID	Particle size, μm ,	Particle size, μm	Particle size, μm	Bulk density, lb/in ³
	d10	d50	d90	
VX 11	3.8	13.7	33.3	0.095
VX 12	2.9	11.6	30.9	0.095
VX 13	3.1	9.9	26.9	0.096
VX 14	3.1	11.4	29.6	0.096
VX 15	2.7	10.3	28.3	0.095



(a)



(b)

Figure 4: (a) SEM micrograph of VX-15/15 vol.% SiC DRA showing reasonably uniform distribution of SiC in aluminum alloy matrix and (b) microstructure of VX-15 alloy showing $\text{Al}_3(\text{Sc,Gd,Zr})$ precipitate. Note the size of $\text{Al}_3(\text{Sc,Gd,Zr})$ precipitate is around 100-200 nm.

Table 2 includes the tensile properties data of five DRA materials containing SiC particle as reinforcement at -320F (liquid nitrogen), 75F (air), and 75F (gaseous hydrogen). The pressure for gaseous hydrogen tests was maintained at 5 ksi. The yield strengths of these DRA materials range from 90-101 ksi and ultimate tensile strength range from 93-111 ksi depending on test temperatures and alloy compositions. These strengths are significantly higher than the strength of commercial DRA 6092Al/SiC available today. The strength of DRA is higher at cryogenic temperatures as expected. The modulus of DRA is around 14-15 msi that is consistent with 15% volume loading of SiC particles [23-24]. The lower modulus of DRA in gaseous hydrogen environment appears to be related with smaller sample size rather than hydrogen effect.

Table 2: Tensile properties of DRA containing SiC particles in different environment

Material ID	Test Environment	Temperature, F	Modulus, GPa	Yield Strength, ksi	Tensile Strength, ksi	Elongation, %	Reduction in Area, %
VX11/SiC	LN ₂	-320	14.6	101.4	111.4	0.9	0.9
	Air	75	14.6	93.2	99.8	1.8	2.9
	GH ₂ , 5 ksi	75	9.7	95.2	101.6	1.9	2.4
VX12/SiC	LN ₂	-320	14.4	85.9	97.6	0.2	0
	Air	75	14.2	96.8	100.7	1	2
	GH ₂ , 5 ksi	75	9.7	99.1	102.5	1.3	4.3
VX13/SiC	LN ₂	-320	14.7	90.8	96.8	0.3	0.5
	Air	75	14.4	91.1	94.4	1.1	3.1
	GH ₂ , 5 ksi	75	9.9	93.7	96.8	1.5	3.2
VX14/SiC	LN ₂	-320	15	99.4	104.3	0.4	0.6
	Air	75	14.2	89.9	92.4	0.6	0.9
	GH ₂ , 5 ksi	75	9.7	91.5	94.3	1.4	2.5
VX15/SiC	LN ₂	-320	14.5	99.4	106.6	0.9	1.1
	Air	75	14.2	89.9	92.9	1.5	3.9
	GH ₂ , 5 ksi	75	9.7	91.2	93.8	1.6	2.8

Since limited sample size did not allow us to use standard fixture for carrying out tensile tests in gaseous hydrogen, the modulus data in hydrogen appears to be inaccurate. The ductility of DRA materials is generally low at different temperatures with lowest one at -320F. The lower ductility is due to following: (a) the presence of angular SiC particles, and (b) an unoptimized processing. In order to provide a comparison for alloy compositions in different environments, extrusion temperature of DRA was kept constant at 662F.

Table 3: Tensile properties of DRA containing B₄C particles in different environment

Material ID	Test Environment	Temperature, F	Modulus, GPa	Yield Strength, ksi	Tensile Strength, ksi	Elongation, %	Reduction in Area, %
VX11/B ₄ C	LN ₂	-320	14.5	99.9	110.9	1.2	0.9
	Air	75	13.8	91.9	97.7	1.3	2.4
	GH ₂ , 5 ksi	75	9.6	93.1	99.9	1.8	3.1
VX12/B ₄ C	LN ₂	-320	14.5	98.4	105.1	0.5	0.6
	Air	75	13.9	94.6	99.5	1.3	2.2
	GH ₂ , 5 ksi	75	9.7	96.1	100.6	1.8	2.9
VX13/B ₄ C	LN ₂	-320	14.7	99.3	104.9	0.6	0.9
	Air	75	14.2	91.3	94.6	1.4	3.3
	GH ₂ , 5 ksi	75	9.6	91.8	95.6	1.6	2.9
VX14/B ₄ C	LN ₂	-320	14.3	99.6	104.2	0.4	0.6
	Air	75	13.8	90.4	93.8	1.2	2.6
	GH ₂ , 5 ksi	75	9.7	91.8	94.2	1.5	1.1
VX15/B ₄ C	LN ₂	-320	14.4	96.6	104.7	0.9	1.1
	Air	75	13.5	87.8	91.9	1.6	3
	GH ₂ , 5 ksi	75	9.7	88.2	92.8	2.2	3.5

Table 3 contains tensile properties data for DRA materials with B_4C particles as reinforcement. The yield strength and tensile strength for B_4C reinforced DRA materials are high similar to SiC reinforced DRA. The yield strength of B_4C reinforced DRA range from 88-100 ksi and ultimate tensile strength range from 92-111 ksi. The modulus values are consistent with 15% volume loading of B_4C particles and they are similar to SiC reinforced DRA. The ductility is also low similar to SiC reinforced DRA. It is important to note that both SiC and B_4C reinforced DRA materials showed high strengths in air and gaseous hydrogen indicating good compatibility with hydrogen environment. Good hydrogen resistance of present DRA materials is similar to the behavior of other aluminum alloys.

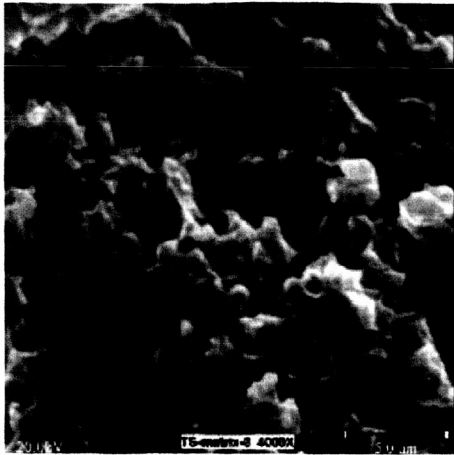
The tensile properties data of matrix aluminum alloys are given in Table 4. These data represent ambient temperature results of matrix alloys that were extruded at different temperatures. While strengths of matrix alloys are slightly lower than DRA materials, ductilities are higher for matrix alloys. This trend is expected because matrix alloys do not contain any reinforcement. The yield strength of matrix alloys range from 84-90 ksi, which is a significant part of strength of DRA suggesting that strength of DRA is primarily controlled by strength of matrix alloy. The data for VX-13 alloy shows that the ductility increased with an increase in the extrusion temperature. This is likely the result of better consolidation at higher extrusion temperature. The moduli of these alloys are slightly higher than commercial aluminum alloys due to presence of Al_3Sc based precipitates. VX-13 and VX-15 alloys showed good combination of strength, 84-87 ksi and ductility, 4.5-6.5%. The data also indicates that the properties of these alloys can be varied considerably with variation in extrusion temperature. A detailed study on the influence of processing parameters on microstructure and properties is needed to understand the deformation behavior of these alloys.

Table 4: Tensile properties of unreinforced aluminum alloys tested at room temperature

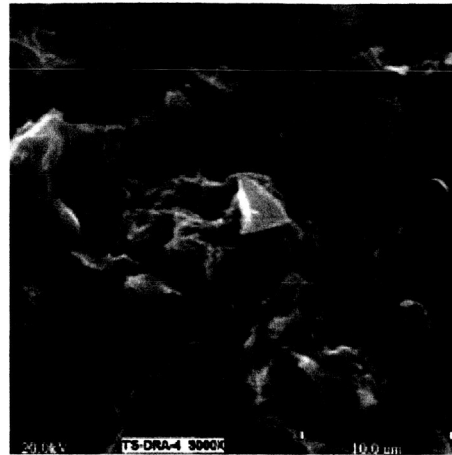
Material ID	Extrusion Temperature, F	Test Temperature, F	Modulus, GPa	Yield Strength, ksi	Tensile Strength, ksi	Elongation, %	Reduction in Area, %
VX11	572	75	9.6	84.9	85.4	2.1	6.6
VX12	662	75	10.1	87.8	89.1	2.1	5.4
VX13	572	75	9.1	86.2	87.2	1.9	6.6
VX13	662	75	9.9	87.1	88.1	1.6	6.3
VX13	752	75	10.5	84.1	88.2	6.5	12.8
VX14	662	75	10.4	90.1	91.1	1.9	6.8
VX15	662	75	10.4	86.8	91.5	4.6	9.5

The yield strength of matrix aluminum alloys can be predicted by solid solution strengthening model, Orowan strengthening, antiphase boundary strengthening and grain boundary strengthening. In order to predict strengthening in DRA materials, load transfer model has to be used in addition to above models. Kendig and Miracle [22] suggested that grain boundary, antiphase boundary and solid solution strengthening models contribute significantly towards strengthening of Al-Sc based alloys.

Figure 5(a)&(b) shows the SEM fractographs of VX-15 matrix alloy and VX-15/SiC DRA. While both materials show ductile failure with microvoid coalescence mechanism, the matrix alloy showed more dimples compared to DRA. DRA fracture surface has shallower dimples with few SiC particles. The presence of SiC particles on fracture surface indicates that SiC fracturing has occurred during deformation of this material that is consistent with previous studies on DRA materials [23-24].



(a)



(b)

Figure 5: SEM micrographs of (a) unreinforced aluminum alloy and (b) VX-15/SiC DRA showing ductile failure controlled by microvoid coalescence mechanism.

Summary and Conclusions

1. The helium gas atomized powder of Al-Mg-Sc-Gd-Zr alloys can be used to produce very fine sized powder with cellular microstructure. The powder was free from primary particles of Al_3Sc .
2. The matrix alloys based on Al-Mg-Sc-Gd-Zr system and DRA materials with SiC and B_4C particles reinforced in matrix alloys were processed using a powder metallurgy process. In order to understand the effect of alloy compositions on the microstructure and tensile properties, processing parameters were held constant in most cases.
3. The microstructure of matrix alloys contains fine Al_3Sc based precipitates, which are very effective for strengthening in these alloys. The microstructure of DRA had uniform distribution of reinforcements in aluminum alloy matrix.
4. DRA materials with SiC and B_4C particles showed very high strengths 88-111 ksi in liquid nitrogen, air and gaseous hydrogen environments compared to commercial DRA. They had excellent resistance in gaseous hydrogen. Lower ductility of DRA was due to presence of reinforcements and inadequate processing.
5. The matrix alloys showed a good combination of strength and ductility in the as-extruded condition. The observed yield strength of these alloys can be explained using solid solution strengthening, Orowan strengthening, antiphase boundary strengthening, and grain boundary strengthening models.

Acknowledgments

This work was performed at Pratt & Whitney Space Propulsion, West Palm Beach, FL under NASA contract NAS8-01108. One of the authors (ABP) would like to thank Chris Rhemer and Thomas Tillman from Pratt & Whitney for helpful discussions.

References

1. M.J. Cooper and R.F. Singer, "Proceeding of Structural Metals by Rapid Solidification" edited by F.H. Froes and S.J. Savage, Orlando, Florida, 1986, p.273.
2. D.S. Skinner, "Dispersion Strengthened Aluminum Alloys" edited by Y-W Kim and W.M. Griffith, TMS Annual Meeting, Arizona, January 1988, p.181.
3. W.M. Griffith, R.E. Sanders, Jr., G.J. Hildman, "High Strength Powder Metallurgy Aluminum Alloys, AIME, 1982, p. 209.
4. Y-W Kim, "Dispersion Strengthened Aluminum Alloys" edited by Y-W Kim and W.M. Griffith, TMS Annual Meeting, Arizona, January 1988, p.157.
5. C.M. Adam and R.G. Bourdeau, "Rapid Solidification Processing" edited by R. Mehrabian et al., Baton Rouge, 1980, p.246.
6. I.G. Palmer, M.P. Thomas and G.J. Marshall, "Dispersion Strengthened Aluminum Alloys" edited by Y-W Kim and W.M. Griffith, TMS Annual Meeting, Arizona, 1988, p.217.
7. M.E. Fine, "Dispersion Strengthened Aluminum Alloys" edited by Y-W Kim and W.M. Griffith, TMS Annual Meeting, Arizona, January 1988, p. 103.
8. W.E. Frazier and M.J. Koczak, "Dispersion Strengthened Aluminum Alloys" edited by Y-W Kim and W.M. Griffith, TMS Annual Meeting, Arizona, January 1988, p. 573.
9. K.S. Chan, "Dispersion Strengthened Aluminum Alloys" edited by Y-W Kim and W.M. Griffith, TMS Annual Meeting, Arizona, January 1988, p. 283.
10. E. Bouchand, L. Kubin, and H. Octor, Metall. Trans. A, 22A, 1990, p. 1021.
11. D.S. Skinner, M.S. Zedalis, and P. Gilman, Mater. Sci. Eng., 119A, 1989, p. 81.
12. R.R. Sawtell and C.L. Jensen, Metall. Trans. A, 21A, 1990, p. 421.
13. L.S. Toropova, D.G. Eskin, M.L. Kharakterova and T.V. Dobatkina, "Advanced Aluminum Alloys Containing Scandium: Structure and Properties" Gordan and Breach Science Publishers, Moscow, Russia.
14. M.E. Drits, L.S. Tropova and Yu.A. Bykov, Metallovedenie. I Termcheskaya, Obbrabotka Metallov., 7, 1983, p. 60.
15. N. Blake and M.A. Hopkins, J. Mater. Sci., 20, 1985, p. 2861.
16. R.W. Hyland, Metall. Trans. A, 23A, 1992, p. 1947.
17. R.R. Sawtell and J.W. Morris, Jr., "Dispersion Strengthened Aluminum Alloys", edited by Y-W. Kim and W.M. Griffith, TMS Meeting, 1988, p. 409.
18. B.A. Parker, Z.F. Zhou and P. Nolle, J. Mater. Sci., 30, 1995, p. 452.
19. R. Unal and K.U. Kainer, Powder Metallurgy, 41, 1998, p.119.
20. A. B. Pandey, K.L. Kendig and D.B. Miracle, "Affordable Metal-Matrix Composites For High Performance Applications" edited by Pandey et al., TMS Meeting, Indianapolis, IN, 2001, p. 35.
21. L.A. Willey, "Physical Metallurgy Division Report, 13-62-EH3" (Alcoa Laboratories 1962).
22. K.L. Kendig and D.B. Miracle, Acta Mater., 50, 2002, 4165.
23. A.B. Pandey, B.S. Majumdar and D.B. Miracle, Metall. Trans. A, 29A, 1998, 1237.
24. A.B. Pandey, B.S. Majumdar and D.B. Miracle, Metall. Trans. A, 31A, 2001, 921.